Materials International
Open-Access Journal (ISSN: 2668-5728)

Article
Volume 7, Issue 4, 2025, 37
https://doi.org/10.33263/Materials74.037

Design and Release Study of Polymeric Nanoparticles of Anti-Hyperlipidemic Agent- Rosuvastatin and Drug Polymer Interaction

Ranu Chaturvedi [1,*]

[1] Department of P.G. Studies and Research in Chemistry and Pharmacy, Rani Durgavati University, Jabalpur 482001, M.P., India
* Correspondence: drranuchemrdvv@gmail.com;

Received: 30.05.2025; Accepted: 10.11.2025; Published: 10.12.2025

Abstract: The relevance of nanoparticle synthesis in several fields is well-known due to its important physical and chemical properties. Statins, anti-hyperlipidemic agents, are known to contribute to cardiovascular protection by improving endothelial function, stabilizing plaques, and exerting anti-inflammatory and anti-thrombotic effects. Biocompatibility, biodegradability, solubility, and non-toxicity make polyvinylpyrrolidone (PVP) safe, and it is widely considered in medicine, cosmetics, pharmaceuticals, and biomedical applications. With this background, in the present study, polymeric rosuvastatin nanoparticles have been synthesized and characterized by FTIR, XRD, and EDSSEM data. The broad band in the 3700 - 2900 cm^{-1} exhibited the highest integrated area (85.35), confirming strong hydrogen bonding due to hydroxyl groups. The average microstrain and average crystallite size obtained is 0.334% and 31.94 nm, respectively, indicating moderate lattice distortion and semicrystalline nature of the polymer. The kinetic release mechanism of rosuvastatin nanoparticles follows zero-order kinetics and the Korsmeyer−Peppas model. The lower AIC of -25 justified the Korsmeyer-Peppas model as the best fit to describe the drug release kinetics. The n values (0.93 and 0.98) indicate anomalous transport with a dominant polymer relaxation component, approaching the characteristics of supercase II transport. This suggests that the rate-limiting step for drug release is the relaxation of the polymer matrix. Such release formulations reduce the side effects and improve patient compliance. It was observed that the percentage release of rosuvastatin was increased considerably through nanoparticle formulation, implying its significance in release kinetics. Avogadro's software, available online, is used for the visualization of the molecular structure of ROSNPs.

Keywords: Rosuvastatin; release kinetics; synthesis; characterization; nanoparticles.

1. Introduction

Drug delivery systems based on nanotechnology, predominantly involving polymeric nanoparticles, have attracted substantial attention as an effective strategy to enhance solubility, stability, and controlled release of poorly soluble drugs. In the present system, nanoparticles of the antihyperlipidemic agent rosuvastatin are synthesized and characterized, and serve as a sample for studying release kinetics. Rosuvastatin (3R,5R)-7-[4-(4-fluorophenyl)-2-(methyl-methylsulfonyl-amino)-6-propan-2-yl-pyrimidin-5-yl]-3,5-dihydroxy-heptanoic acid with a chemical formula of $C_{22}H_{30}FN_3O_6S$ is a lipid-lowering drug that reduces the amount of

cholesterol by slowing the production of cholesterol in the liver [1-3] and provides cardiovascular protection by improving endothelial function, plaque stabilization, anti-inflammatory, and anti-thrombotic effects [4,5]. Statin therapy, at early stages, is considered proportional to LDL reduction [6] and is one of the best approaches for treating cardiovascular complications [7, 8]. Triglyceridemia, as well as Homozygous Familial Hypercholesterolemia, is treated with rosuvastatin as specified in the FDA Canada monograph [9,10]. Despite its significant therapeutic properties, as mentioned, rosuvastatin exhibits poor aqueous solubility and low bioavailability, necessitating high doses to maintain effective plasma concentrations. Thus, the advancement from conventional to novel delivery systems that enhance solubility and maintain drug stability is essential. Polymeric nanoparticles are efficiently used to improve the encapsulation efficiency and controlled release. With this view, polyvinylpyrrolidone (PVP), also called polyvidone or povidone, which has strong binding properties, outstanding solubility in solvents of various polarities, and which improves the physicochemical properties of drugs [11,12], is used. The properties, such as biocompatibility, biodegradability, solubility, and non-toxicity, make it safe by the Food and Drug Administration (FDA) and are widely considered in medicine, cosmetics, pharmaceuticals, and biomedical applications. PVP is used to improve the development of a drug delivery system for oral, topical, transdermal, and ocular administration [13-16]. Since PVP produced a little larger drug loading (78%) than the uncoated nanoparticles, numerous active chemicals from various categories have been added to PVP microparticles and nanoparticles [17,18]. As reported, the molecular framework and hydrophilic nature of polyvinyl alcohol (PVA) make it suitable to be employed as a granulating liquid to limit crystal formation, stop nucleation, as well as to get rid of excess water by absorption [19]. PVA microspheres are used to deliver drugs by encapsulating different therapeutic agents [20] and are frequently used as excipients in medications that are delivered transdermally, vaginally, and ophthalmically. PVA and PVP, together in pharmaceutical additive manufacturing, have a remarkable influence [21].

In this study, rosuvastatin drug nanoparticles (ROSNPs) were selected to be encapsulated in the PVP core, and PVA was used as a stabilizer. Synthesis of NPs from rosuvastatin and PVP is accomplished with the research objective to improve (i) drug dissolution rate through size reduction and by providing a hydrophilic microenvironment around the drug; (ii) encapsulation efficiency (EE), which indicates the proportion of drug successfully entrapped within the polymeric matrix. High EE (95%), as observed in the present study, is crucial for maintaining therapeutic dosage and achieving sustained release; (iii) to understand the mechanism of sustained release of ROSNPs. It is hypothesized that the synthesized nanoparticles from rosuvastatin and PVP will exhibit improved solubility and high encapsulation efficiency due to molecular interactions between the drug and the polymer. In addition, drug release kinetics are hypothesized to follow a diffusion-controlled mechanism along with relaxation of the polymer matrix, leading to the sustained release.

2. Materials and Methods

2.1. Sample preparation.

Rosuvastatin, available on the market under the brand name Vivier Pharma Private Limited, is used as the active compound for nanoparticle formulation, while polyvinylpyrrolidone (PVP), purchased from Thomas Baker Laboratories, serves as the polymer matrix to encapsulate the nanoparticles. Dimethyl sulfoxide acts as the solvent,

facilitating the dissolution of both PVP and rosuvastatin during the preparation process. To stabilize the nanoparticle dispersion and prevent agglomeration, polyvinyl alcohol (PVA) purchased from Thomas Baker is employed. A dialysis membrane is used to enable controlled release. Phosphate-buffered saline (PBS) is selected as the release medium for conducting in vitro studies to simulate physiological conditions.

Solution of Rosuvastatin was prepared by dissolving 20 mg of rosuvastatin in 10 mL DMSO. 1% (w/v) Polyvinylpyrrolidone (PVP, Mol. Wt. = 40,000 g/mol) solution was prepared separately in 10% DMSO. 2% (w/v) solution of Polyvinyl alcohol (PVA, Mol. Wt.= 125,000 g/mol) was prepared in double-distilled water. The drug-polymer solution was prepared by mixing 10 mL drug solution containing 20 mg rosuvastatin with 8 ml, 1% (w/v) PVP containing 80 mg PVP, yielding a final concentration of 1.11 mg/mL of rosuvastatin and 4.44 mg/mL PVP in the drug -polymer mixture corresponding to a 1:4 (w/w) drug-polymer ratio. Drug-polymer solution was added to 10 mLof 1% PVA solution dissolved in 50 mL of water positioned on the magnetic stirrer for the nanoparticles formation. Stabilizer, Polyvinyl alcohol, prevents agglomeration of prepared nanoparticles. The suspension was centrifuged at 10,000 rpm for 20 minutes to collect the nanoparticles.

The encapsulation efficiency was determined by measuring the concentration of the free drug in the supernatant using the formula:

$$\% EE = \frac{MASS\ OF\ ENTRAPPED\ DRUG}{TOTAL\ MASS\ OF\ DRUG\ ADDED} \times 100 \quad (1)$$

% Encapsulation efficiency was found to be 95%. These synthesized nanoparticles are characterized by using FTIR, XRD, and EDSSEM. The FTIR spectrum was recorded using an FTIR spectrophotometer, FTIR-8400 (Shimadzu, Japan), in the range of 4000-400 cm^{-1}. Samples were prepared by the KBr pellet method. X-ray diffraction (XRD) patterns were obtained by using an X-ray diffractometer model Miniflex 600 (Rigaku, Japan) equipped with Cu Kα radiation (λ = 1.5406 Å), scanning within the 2θ range of 10°–80°. Scanning Electron Microscopy (SEM) and Energy-Dispersive Spectroscopy (EDS) analysis were performed using an FEI Nova Nano SEM 450 and a Bruker XFlash6130, respectively. SEM images were obtained at an accelerating voltage of 15 kV, and elemental composition was determined through EDS point analysis and mapping. Avogadro's software, available online, is used for the visualization of molecular structure, not for structural validation.

2.2. Measurement techniques.

ROSNPs (1 mg) were dispersed in 5 mL of PBS (pH 7.4) and positioned into the dialysis bag. This dialysis bag was set into 100 mLof aqueous recipient medium of PBS placed on the stirrer at 300 rpm at 37°C, and then the samples were released continuously and withdrawn at specific time intervals, i.e., at 2, 10, 30, 45, 60, 72, 80, 110, 133, 188, 193, and 210 minutes and then after 24 hours, to measure the release profiles and analyzed by using a UV-Visible Spectrophotometer. The same volume (5 ml) of fresh PBS was added to maintain the sink condition. This setup facilitates the controlled release of rosuvastatin nanoparticles through the membrane, enabling precise measurement of the release profile during the study (Figure 1).

2.3. Analysis method.

The release kinetics of the ROSNPs were followed spectrophotometrically by absorbance measurements using a Thermo Scientific UNICAM UV–Vis 500 spectrophotometer. A calibration curve for rosuvastatin was constructed for different dilutions prepared from a stock solution of rosuvastatin. The calibration curve following Beer's law was established by measuring the absorbance at 258.5 nm. Absorbance was measured using a UV-Visible Spectrophotometer at different time points, as reported, to determine the released ROSNPs. The UV-Vis calibration curve showed good linearity with a correlation coefficient R^2 = 0.9936. The limit of detection (LOD) and limit of quantitation (LOQ) were 0.088 and 0.268 mg/ml, respectively. The LOQ/LOD ratio is 3.07, which is consistent with the calibration-curve approach.

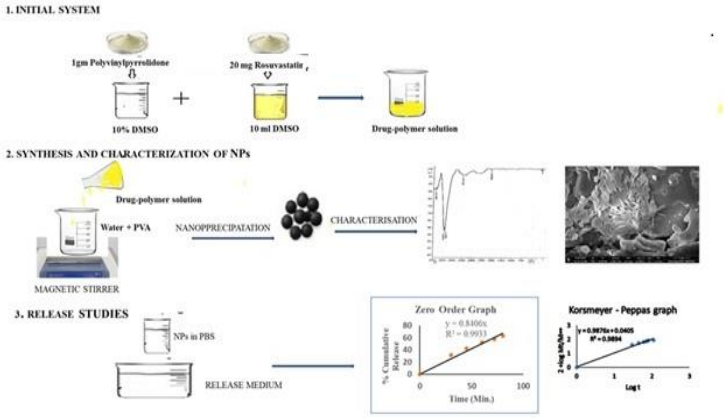

Figure 1. Schematic representation of nanoparticle preparation and steps of release kinetics. Step 1 - Preparation of Rosuvastatin-PVP solution followed by Step 2, synthesis of ROSNPs by nano-precipitation method and characterization by FTIR, SEM. Step 3: release kinetic studies of ROSNPs using PBS as the release medium.

The release data obtained from these analyses are used to construct drug release profiles. Mathematical models such as zero-order, first-order, Higuchi, and Korsmeyer-Peppas are applied to quantitatively understand release kinetics [21], allowing rate constants for each model to be evaluated. Research indicates zero-order kinetics along with Korsmeyer-Peppas behavior up to sixty percent of drug discharge. The model proposed by Korsmeyer–Peppas includes a semi-empirical equation, as given below, to elucidate the release of the drug from the systems involving polymeric structures.

$$M_t / M_\infty = k.t^n \qquad (2)$$

Where the Mt and M∞ represent the amount of rosuvastatin nanoparticles released at time t ∞, respectively, the release rate constant is k, and n is the release exponent, which indicates the mechanism of drug release. The release exponent is found to be greater than 0.89, highlighting the super case II transport for which rate and time are related as t^{n-1} [22], and the system involves diffusion along with relaxation of polymer chains [23].

3. Results and Discussion

3.1. Kinetic studies.

The maximum absorbance (λmax) of rosuvastatin is obtained at 258.5 nm. The linear regression coefficient of 0.9936 confirms the validity of the Beer-Lambert law, from which the

concentrations at different time intervals and the corresponding percentage cumulative release have been calculated (Table 1). Absorbance and concentration values are presented along with standard deviations (n=3), while percentage cumulative release was calculated from the mean concentration.

Table 1. *In vitro* drug release data showing calculated concentration, percentage cumulative release with respect to time.

Sl. No.	Time (Min)	Absorbance ± 0.01455	Concentration (mg/ml) ± 0.009169	Percentage cumulative release (%)
1	0	0	0	0
2	2	0.4	0.02	10.5
3	10	0.72	0.04	21.1
4	30	0.73	0.06	31.6
5	45	1.2	0.08	42.1
5	60	1.56	0.10	52.6
6	72	1.62	0.11	57.9
7	80	1.68	0.12	63.2
8	110	1.80	0.13	68.4
9	133	1.95	0.15	78.9

Percentage cumulative release data is used to formulate a zero-order plot (Figure 2). The regression coefficient is found to be 0.98, which clearly shows the applicability of zero-order kinetics. The release rate constant (K_0) was 0.8406 ± 0.0309 %·h^{-1}. Zero-order kinetics has also been confirmed by using a conventional zero-order equation. After almost 60 percent of the drug is released, the order changes from zero to one.

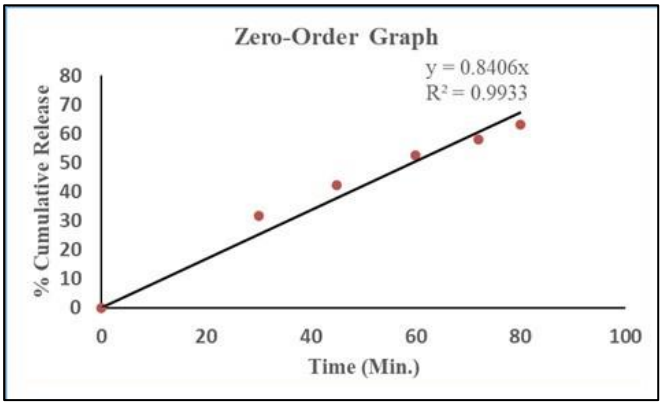

Figure 2. Zero-order kinetics of ROSNPs. The % cumulative release increases linearly with time, indicating zero-order reaction behavior. The slope corresponds to the rate constant k.

A matrix formulation for the present system was identified by fundamental mathematical models. The result indicates that release kinetics does not follow normal Higuchi's criteria for drug release up to 60 percent drug release. However, the polynomial of order 2 trendline is evident in the Higuchi plot, indicating complex, nonlinear dynamics in the underlying system. The Korsmeyer-Peppas model (Table 2) was followed by plotting Log cumulative percentage release vs. log t and log Mt/M∞ vs. log t with regression coefficients of 0.9909 and 0.989, respectively (Figures 3 and 4).

Table 2. Korsmeyer – Peppas Constant using log percentage cumulative release and log Mt/M∞ vs. log t.

Sl. No.	Time (Min.)	Log percentage cumulative release	log t	Mt/M∞	Log Mt/M∞	2 + log Mt/M∞
1	0	0	0	0	0	0
2	2	1.02	0.30103	0.133	-0.87615	1.123852
3	10	1.32	1	0.267	-0.57349	1.426511
4	30	1.499	1.477121	0.4005	-0.3974	1.602603

Sl. No.	Time (Min.)	Log percentage cumulative release	log t	Mt/M∞	Log Mt/M∞	2 + log Mt/M∞
5	45	1.62	1.653213	0.5335	-0.27287	1.727134
6	60	1.72	1.778151	0.6666	-0.17613	1.823865
7	72	1.76	1.857332	0.734	-0.1343	1.865696
8	80	1.8	1.90309	0.801	-0.09637	1.903633
9	110	1.83	2.041393	0.866	-0.06248	1.937518

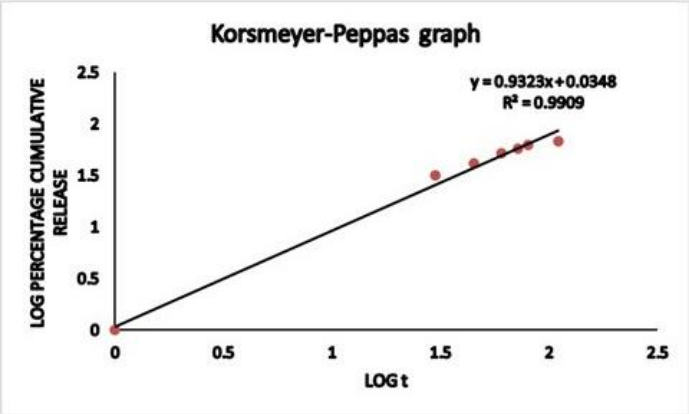

Figure 3. Korsmeyer-Peppas kinetic model for ROSNPs, plotted as log percent cumulative release vs. log t. The plot indicates the linear region, indicating super-case II transport mechanism. The slope gives the release exponent n, while the intercept provides log k.

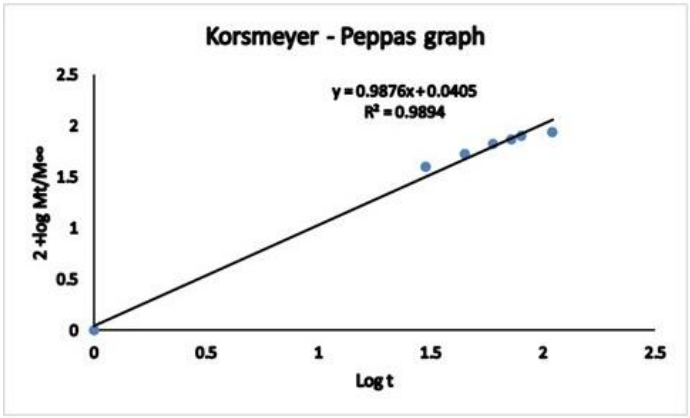

Figure 4. Korsmeyer-Peppas release kinetics for ROSNPs between Log(Mt/M∞) and Log t. Plot of log (Log(Mt/M∞) vs. Log t showing the linear region used to determine the release exponent n and kinetic constant k. The slope gives the release exponent n, while the intercept provides log k.

The Korsmeyer-Peppas power law equation predicts that the fractional release of the drug is exponentially related to the release time. This method is commonly used for polymeric systems, and the values of K and n are calculated to be approximately 1 and above 0.9, respectively, for the best fit. Since both the approaches, i.e., normalized form log (Mt/M∞) vs. log t and log of cumulative percentage release vs. log t (Figures 2 and 3), yielded similar values for the release exponent n and the kinetic constant K, the results are considered consistent and reliable. The similarity between the two approaches reinforces the robustness of the model fit to our formulation data. The fitting parameters, along with the comparative statistical measures, i.e., adjusted R^2, root mean square error (RMSE), and the Akaike information criterion (AIC), are summarized in Table 3.

Table 3. Comparative statistical data of kinetic models.

Order/model	K	N	R^2	Adjusted R^2	RMSE	AIC
Zero O=order	K=0.8406 ±	-	0.9938	0.9835	4.16	15.139

	0.0309%·h^{-1}					
Korsmeyer-Peppas model						
1.Log cumulative percentage release vs. log t	k=1.0839± 0.066 min$^{-0.93}$	0.93±0.03987	0.9909	0.9636	0.06823	-25.4
2. log Mt/M∞ vs. log t	1.096±0.0758 min$^{-.0.98}$	0.98±0.04565	0.9894	0.9578	0.078	-24.05

Both models demonstrate high correlation coefficients (R2); the adjusted R2 of 0.9835 for the zero-order model and slightly lower values —0.9636 and 0.9578—for the Korsmeyer-Peppas model indicate the goodness of fit for the zero-order model. However, the lower AIC supported the Korsmeyer-Peppas model as the best fit for describing the drug release kinetics. The release exponent, n = 0.93/0.98, indicates anomalous transport approaching case II/supercase II transport in polymeric systems. This suggests that the rate-limiting step for drug release is the relaxation of the polymer matrix along with diffusion.

3.2. Qualitative and quantitative analysis.

In the present study, polymeric nanoparticles have been prepared and characterized by using FTIR, XRD, and EDSSEM data.

3.2.1. Qualitative analysis -FTIR.

The FTIR spectrum (Figure 5) using a KBr pellet was recorded in the range 450 cm^{-1}–4000 cm^{-1}. Broad absorption around 3400 cm^{-1} is due to O-H stretching of the PVP hydroxyl group. The peaks at 2900 cm^{-1} and 1650 cm^{-1} correspond to C-H stretching and C=O stretching, respectively, which are prominent in the lactam group of PVP and carbonyl group in ester. Peaks at 1280-1000 cm^{-1} could be due to C-N or C-O stretching common in PVP and ester functional groups in statins. Predominant FTIR bands are obtained at 3884.76, 3404.47, 2617.49, and 1629.90 cm^{-1}, clearly revealing the interaction of the constituents, potential changes in drug crystallinity, and involvement of different functional groups in the formation of ROSNPs. Avogadro's software, available online, is used for molecular visualization, not for structural validation of ROSNPs based on FTIR analysis (Figure 6).

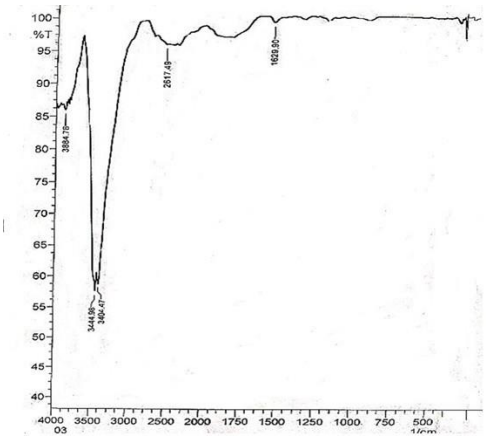

Figure 5. FTIR spectrum of synthesized ROSNPs. The spectrum, recorded in transmittance mode, confirms the successful synthesis. Key vibrational modes include the strong O-H stretching band at around 3400 cm^{-1}, C-H stretching at 2900 cm^{-1}, and C=O stretching at 1650 cm^{-1}, which are prominent in the lactam group of PVP and carbonyl group in ester.

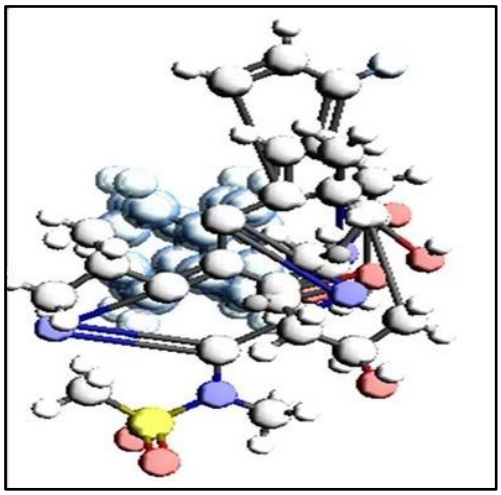

Figure 5. Structure of ROSNPs. The 3D optimized structure of ROSNPs, visualized using Avogadro. The molecule is shown in a Ball-and-Stick representation, with carbon atoms black, oxygen red, hydrogen white, nitrogen dark blue, and sulfur yellow.

3.2.2. Quantitative analysis -FTIR.

Quantitative FTIR analysis was performed by analyzing the baseline-corrected FTIR spectrum of the sample in the range of 4000-400 cm^{-1} and then integrating the area under peaks using Excel. The peak areas corresponding to the major functional groups were determined to evaluate the relative abundance and chemical interaction in the sample. The band around 3700-2900 cm^{-1} exhibits the highest integrated area (85.35), indicating the maximum interaction of hydroxyl groups. Peak areas around 3800-4000, 1600-1800, 1400-1600, 1000-1300, and 950-650 cm^{-1} are found to be 27, 16.94, 27.99, 37, 43.4, and 47.32, respectively. The increase in the peak areas of the carbonyl and hydroxyl bands suggests enhanced interfacial interactions and possible oxidation during the synthesis of nanoparticles from rosuvastatin and the polymer. Thus, the quantitative FTIR results are similar to the qualitative observations and support chemical modification of the matrix.

3.2.3. Quantitative analysis-XRD.

Quantitative analysis of XRD studies was carried out using Bragg's relation and the Scherrer formula. The sample shows reflections at 2θ = 15.86°, 38°, 44°, 64°, and 77°, yielding d-spacings in the range of 1.237-5.583Å. After converting the FWHM values to radians, the coherent scattering domain was found to lie between 25 and 40nm. The average microstrain obtained from peak broadening is 0.00334 (0.334%), indicating moderate lattice distortion, consistent with the semicrystalline nature of the polymer. The average crystallite size of the particles is 31.94 nm, as calculated from Scherrer's formula. These results confirm that the polymer contains nanocrystalline regions dispersed within an amorphous phase.

3.2.4. EDS analysis.

To authenticate the ROSNPs' formation, EDSSEM analysis was performed. The EDS report shows a carbon- and oxygen-rich sample with minor contributions from elements such as aluminum, potassium, and calcium, suggesting that the sample characteristics are similar to those of a biologically derived sample (Table 4). It is pertinent to note that although rosuvastatin and PVP do not contain sodium or chloride in their chemical composition, the relatively high percentages of Na and Cl observed in the EDS analysis are attributed to surface-

level contamination rather than the bulk material composition. Since EDS is a surface-sensitive technique, any residual salts or handling-related contamination can contribute significantly to the detected elemental percentages, even when absent in the actual formulation.

Table 4. EDS analysis.

El	AN	Series	unn. C [wt.%]	norm. C [wt.%]	Atom. C [at.%]	Error (1 sigma) [wt.%]
Cl	17	K-series	29.60	43.68	28.25	1.03
Na	11	K-series	21.89	32.30	32.21	1.41
C	6	K-series	9.42	13.90	26.54	2.77
O	8	K-series	5.17	7.63	10.93	1.24
Al	13	K-series	1.18	1.74	1.48	0.10
Si	14	K-series	0.43	0.64	0.52	0.06
Ca	20	K-series	0.08	0.12	0.07	0.04
Au	79	M-series	0.00	0.00	0.00	0.00
Total			67.77	100.00	100.00	

3.2.5. SEM analysis.

SEM images of ROSNPs are shown in Figure 7. The particles appear to be crystalline, exhibiting distinct facets and edges that vary in size and shape, with some appearing needle-like and growing from a central point. The surface appears relatively smooth, providing a contrast to the rough texture of the particles, confirming the particles' almost circular shape, smooth surfaces, and well-separated surfaces.

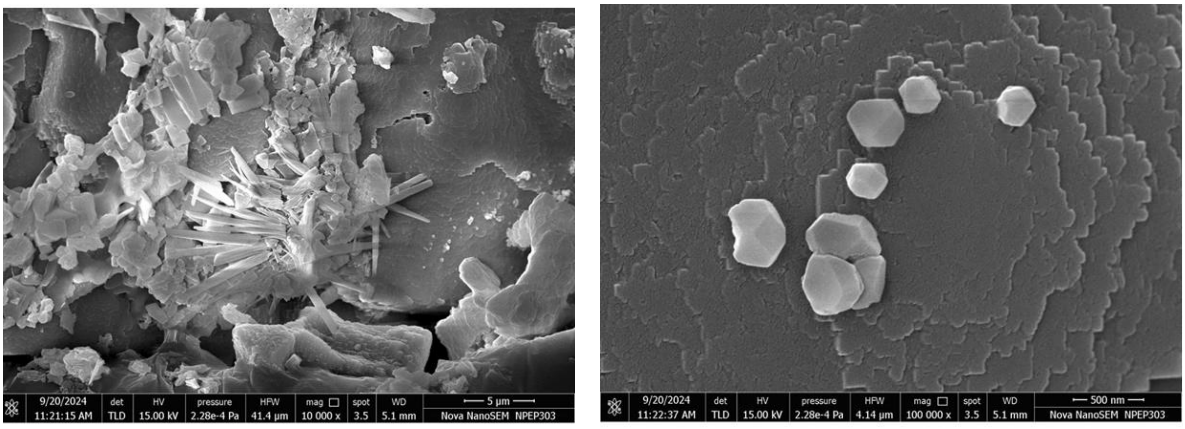

Figure 7. SEM images of ROSNPs. Micrographs display needle-like crystals growing from a central point. The surface appears relatively smooth, providing a contrast to the rough texture of the particles. The image was acquired using secondary electron detection at an accelerating voltage of 15.00kV and the magnification of x10000 and x100000.

Quantitative analysis of SEM micrographs using ImageJ software revealed morphological features consistent with a nanostructured surface. For the low magnification SEM image (5 µm scale bar), ImageJ analysis detected 6836 individual fragments with a total particle area of 188.86 µm² and an average particle area of 0.028 ± 0.004 µm². Approximately 51.8 ± 2.4% of the surface area was occupied, reflecting the sample's heterogeneous, shattered morphology. In contrast, for the high magnification SEM image (500 nm scale bar), ImageJ analysis identified 106 discrete particles in the micrograph. The total measured particle area was 6.53 x 10^6 µm², with an average particle area of 6.16 x 10^4 µm². These particles covered 93.58% of the image field. Histogram analysis showed a mean gray value of 255, confirming a clear contrast between the particles and the background intensity. Area measurements of individual particles ranged from 54.77 to 63.90 µm², indicating a narrow size distribution, and the gray-scale histogram showed a unimodal pattern with a mean intensity of 83.44, further supporting a broad intensity distribution and high surface brightness across the sample.

3.3. Discussion.

The cumulative release profile of ROSNPs showed a near-uniform increase over time, with almost 70% of the rosuvastatin released in the first 110 min. The absence of a pronounced burst phase indicates that the drug was largely entrapped within the polymer-nanoparticle network rather than loosely bound to the surface. The hydrophilic nature of the polymer blend, PVP/PVA, facilitated consistent medium penetration and polymer swelling, maintaining a steady diffusion rate throughout the release period. For the Korsmeyer-Peppas model (R^2=0.988), the release exponent is above 0.9, indicating non-Fickian transport in addition to dominating polymer relaxation and swelling. This value, close to unity, suggests that polymer chain disentanglement and matrix relaxation played a significant role in sustaining drug release alongside diffusion. The simultaneous fit to the zero-order model also supports the polymer relaxation mechanism, as it facilitates a nearly constant release rate over time. This behavior aligns with previous findings in polymeric microsphere systems, where n = 0.85 also corresponded to combined diffusion-relaxation control and was supported by both the zero-order model [24] and the Korsmeyer-Peppas model [25]. Recently, nanogels of rosuvastatin have been formulated using the hydrophilic polymers β-cyclodextrin (β-CD) and Poloxamer-407 (P407), combined with the monomer 2-acrylamido-2-methylpropane sulfonic acid (AMPS) [26] for solubility enhancement. Nanomaterial-supported molecularly imprinted polymer/receptor-like sensors are developed for the detection of rosuvastatin from binary mixtures [27]. Release kinetics of rosuvastatin calcium using cyclodextrin-based nanocarriers/nanosponges followed zero-order and Higuchi diffusion mechanisms, as reported in recent studies [28]. This again highlights that the mechanism of drug release kinetics is greatly influenced by the type and nature of the polymer used. However, it is pertinent to mention here, to the best of my knowledge, that similar PVP/PVA-based rosuvastatin delivery systems have not been discussed so far. Release profiles currently obtained show constant release rates over time, which are considered ideal for sustained-release formulations and improve patient compliance. The interaction between the drug and the polymer is clearly revealed by the prominent additional bands in FTIR.

4. Conclusion

The study highlights the synthesis of polymeric nanoparticles of the anti-hyperlipidemic agent rosuvastatin, which were characterized by FTIR, SEM, and EDX, followed by release kinetics using diverse reported models, from which release constants were calculated. FTIR confirmed the compatibility of rosuvastatin with PVA and the successful encapsulation of the drug (95%), while SEM micrographs revealed the nanoparticle morphology and size distribution. Dual-magnification SEM, supported by ImageJ quantification, demonstrated that the sample exhibits heterogeneous morphology, containing both highly fragmented micro-particles and well-defined polygonal crystals. The presence of two distinct structural regions within the sample highlights its mixed crystallinity and variable structural integrity. Such nanoparticle formulations undoubtedly improve drug release rates and, hence, have attracted considerable attention worldwide. The present formulation followed zero order and the Korsmeyer-Peppas model, governed primarily by polymer relaxation as indicated by n values (0.93 and 0.98), confirming a transition from case II to super case II mechanism of drug release with a substantial increase in the percentage release of nanoparticles of rosuvastatin as compared to the release of the pure drug. The type of polymer and the method

of preparation play crucial roles in the performance of these systems. In this investigation, a standard polymer and a straightforward technique were employed. Such nanoparticle formulations provide significant advancements in the pharmaceutical industry, particularly as the current formulation is expected to improve the drug's efficacy, consequently lowering the risk of cardiovascular diseases. The current study was limited to in vitro release, which does not account for all physiological factors; thus, in vivo bioavailability and stability studies are necessary to validate the practical application of the formulation.

Author Contributions

Validation, R.C.; formal analysis, R.C.; investigation, R.C.; writing—original draft preparation, R.C.; writing—review and editing, R.C. All authors have read and agreed to the published version of the manuscript.

Institutional Review Board Statement

Not applicable.

Informed Consent Statement

Not applicable.

Data Availability Statement

Data supporting the findings of this study are available upon reasonable request from the corresponding author.

Funding

This research received no external funding.

Acknowledgments

The author acknowledges the support of the Central Instrumentation Facility, Savitribai Phule Pune University, for providing EDSSEM Analysis.

Conflicts of Interest

The authors declare no conflict of interest.

Abbreviations

The following abbreviations are used in this manuscript:

Abbreviation	Definition
EDS	Energy Dispersive Spectroscopy
FTIR	Fourier Transform Infrared Spectroscopy
PVA	Polyvinyl alcohol
PVP	Polyvinylpyrrolidone
ROSNPs	Rosuvastatin nanoparticles
SEM	Scanning Electron Microscopy
XRD	X-ray Diffraction

References

1. Bajaj, T.; Patel, P.; Giwa, A.O. Rosuvastatin. In StatPearls [Internet]. Treasure Island (FL): Stat Pearls Publishing.
2. Force, U.S.P.S.T. Statin Use for the Primary Prevention of Cardiovascular Disease in Adults: US Preventive Services Task Force Recommendation Statement. *JAMA* **2022**, *328*, 746-753, https://doi.org/10.1001/jama.2022.13044.
3. Usman, N.U.B.; Winson, T.; Roy, P.B.; Tejani, V.N.; Dhillon, S.S.; Damarlapally, N.; Panjiyar, B.K. The Impact of Statin Therapy on Cardiovascular Outcomes in Patients With Diabetes: A Systematic Review. *Cureus* **2023**, *15*, e47294, https://doi.org/10.7759/cureus.47294.
4. Siniscalchi, C.; Basaglia, M.; Riva, M.; Meschi, M.; Meschi, T.; Castaldo, G.; Di Micco, P. Statins Effects on Blood Clotting: A Review. *Cells* **2023**, *12*, 2719, https://doi.org/10.3390/cells12232719.
5. Bucci, T.; Menichelli, D.; Palumbo, I.M.; Pastori, D.; Ames, P.R.J.; Lip, G.Y.H.; Pignatelli, P. Statins as an Adjunctive Antithrombotic Agent in Thrombotic Antiphospholipid Syndrome: Mechanisms and Clinical Implications. *Cells* **2025**, *14*, 353, https://doi.org/10.3390/cells14050353.
6. de Jongh, S.; Lilien, M.R.; op't Roodt, J.; Stroes, E.S.G.; Bakker, H.D.; Kastelein, J.J.P. Early statin therapy restores endothelial function in children with familial hypercholesterolemia. *J. Am. Coll. Cardiol.* **2002**, *40*, 2117-2121, https://doi.org/10.1016/s0735-1097(02)02593-7.
7. Waters, D.D.; Guyton, J.R.; Herrington, D.M.; McGowan, M.P.; Wenger, N.K.; Shear, C. Treating to New Targets (TNT) Study: does lowering low-density lipoprotein cholesterol levels below currently recommended guidelines yield incremental clinical benefit?. *Am. J. Cardiol.* **2004**, *93*, 154-158, https://doi.org/10.1016/j.amjcard.2003.09.031.
8. Durrington, P. Statin Resistance, In Hyperlipidaemia: Diagnosis and Management, 3rd Edition; CRC Press: London, **2007**; https://doi.org/10.1201/b13464.
9. Cholesterol Treatment Trialists' (CTT) Collaborators. Efficacy and safety of cholesterol-lowering treatment: prospective meta-analysis of data from 90 056 participants in 14 randomised trials of statins. *Lancet* **2005**, *366*, 1267-1278, https://doi.org/10.1016/S0140-6736(05)67394-1.
10. Rusdin, A.; Mohd Gazzali, A.; Ain Thomas, N.; Megantara, S.; Aulifa, D.L.; Budiman, A.; Muchtaridi, M. Advancing Drug Delivery Paradigms: Polyvinyl Pyrolidone (PVP)-Based Amorphous Solid Dispersion for Enhanced Physicochemical Properties and Therapeutic Efficacy. *Polymers* **2024**, *16*, 286, https://doi.org/10.3390/polym16020286.
11. Franco, P.; De Marco, I. The Use of Poly(*N*-vinyl pyrrolidone) in the Delivery of Drugs: A Review. *Polymers* **2020**, *12*, 1114, https://doi.org/10.3390/polym12051114.
12. Bothiraja, C.; Shinde, M.B.; Rajalakshmi, S.; Pawar, A.P. Evaluation of molecular pharmaceutical and in-vivo properties of spray-dried isolated andrographolide—PVP. *J. Pharm. Pharmacol.* **2009**, *61*, 1465-1472, https://doi.org/10.1211/jpp/61.11.0005.
13. Martins, R.M.; Pereira, S.V.; Siqueira, S.; Salomão, W.F.; Freitas, L.A.P. Curcuminoid content and antioxidant activity in spray dried microparticles containing turmeric extract. *Food Res. Int.* **2013**, *50*, 657-663, https://doi.org/10.1016/j.foodres.2011.06.030.
14. Rasekh, M.; Karavasili, C.; Soong, Y.L.; Bouropoulos, N.; Morris, M.; Armitage, D.; Li, X.; Fatouros, D.G.; Ahmad, Z. Electrospun PVP–indomethacin constituents for transdermal dressings and drug delivery devices. *Int. J. Pharm.* **2014**, *473*, 95-104, https://doi.org/10.1016/j.ijpharm.2014.06.059.
15. Fogaça, R.; Catalani, L.H. PVP Hydrogel Membranes Produced by Electrospinning for Protein Release Devices. *Soft Mater.* **2013**, *11*, 61-68, https://doi.org/10.1080/1539445X.2011.580411.
16. Diaz del Consuelo, I.; Falson, F.; Guy, R.H.; Jacques, Y. Ex vivo evaluation of bioadhesive films for buccal delivery of fentanyl. *J. Control. Release* **2007**, *122*, 135-140, https://doi.org/10.1016/j.jconrel.2007.05.017.
17. Ramalingam, V.; Varunkumar, K.; Ravikumar, V.; Rajaram, R. Target delivery of doxorubicin tethered with PVP stabilized gold nanoparticles for effective treatment of lung cancer. *Sci. Rep.* **2018**, *8*, 3815, https://doi.org/10.1038/s41598-018-22172-5.
18. Gaaz, T.S.; Sulong, A.B.; Akhtar, M.N.; Kadhum, A.A.H.; Mohamad, A.B.; Al-Amiery, A.A. Properties and Applications of Polyvinyl Alcohol, Halloysite Nanotubes and Their Nanocomposites. *Molecules* **2015**, *20*, 22833-22847, https://doi.org/10.3390/molecules201219884.
19. Zahra, F.T.; Quick, Q.; Mu, R. Electrospun PVA Fibers for Drug Delivery: A Review. *Polymers* **2023**, *15*, 3837, https://doi.org/10.3390/polym15183837.

20. Bianchi, M.; Pegoretti, A.; Fredi, G. An overview of poly(vinyl alcohol) and poly(vinyl pyrrolidone) in pharmaceutical additive manufacturing. *J. Vinyl Addit. Technol.* **2023**, *29*, 223-239, https://doi.org/10.1002/vnl.21982.
21. Barzegar-Jalali, M. Kinetic Analysis of Drug Release From Nanoparticles. *J. Pharm. Pharm. Sci.* **2008**, *11*, 167-177, https://doi.org/10.18433/J3D59T.
22. Lisik, A.; Musiał, W. Conductomeric Evaluation of the Release Kinetics of Active Substances from Pharmaceutical Preparations Containing Iron Ions. *Materials* **2019**, *12*, 730, https://doi.org/10.3390/ma12050730.
23. Varma, M.V.S.; Kaushal, A.M.; Garg, A.; Garg, S. Factors affecting mechanism and kinetics of drug release from matrix-based oral controlled drug delivery systems. *Am. J. Drug Deliv.* **2004**, *2*, 43-57, https://doi.org/10.2165/00137696-200402010-00003.
24. Laracuente, M.-L.; Yu, M.H.; McHugh, K.J. Zero-order drug delivery: State of the art and future prospects. *J. Control. Release* **2020**, *327*, 834-856, https://doi.org/10.1016/j.jconrel.2020.09.020.
25. Heredia, N.S.; Vizuete, K.; Flores-Calero, M.; Pazmiño V, K.; Pilaquinga, F.; Kumar, B.; Debut, A. Comparative statistical analysis of the release kinetics models for nanoprecipitated drug delivery systems based on poly(lactic-co-glycolic acid). *PLOS ONE* **2022**, *17*, e0264825, https://doi.org/10.1371/journal.pone.0264825.
26. Shoukat, H.; Pervaiz, F.; Rehman, S.; Khan, K.U.; Sarfraz, M.; Noreen, S.; Raza, M.R.; Mahmood, H. Enhancing solubility and oral bioavailability of rosuvastatin through interpenetrating polymer network (IPN) nanogels: Fabrication, characterization, and *in-vivo* efficacy assessment. *J. Drug Deliv. Sci. Technol.* **2024**, *98*, 105866, https://doi.org/10.1016/j.jddst.2024.105866.
27. Gharibi, M.; Piskin, E.; Bounoua, N.; Cetinkaya, A.; Ozkan, S.A. Development of nanomaterial-supported molecularly imprinted polymer/receptor-like sensor for the detection of rosuvastatin from binary mixtures. *Talanta Open* **2024**, *10*, 100376, https://doi.org/10.1016/j.talo.2024.100376.
28. Zaki, R.M.; Alfadhel, M.; DevanathaDesikan Seshadri, V.; Albagami, F.; Alrobaian, M.; Tawati, S.M.; Warsi, M.H.; Almurshedi, A.S. Fabrication and characterization of orodispersible films loaded with solid dispersion to enhance Rosuvastatin calcium bioavailability. *Saudi Pharm. J.* **2023**, *31*, 135-146, https://doi.org/10.1016/j.jsps.2022.11.012.

Publisher's Note & Disclaimer